Comparative Medicine
Copyright 2017
by the American Association for Laboratory Animal Science

Vol 67, No 4
August 2017
Pages 300–314

Original Research

Optimization of Glioblastoma Mouse Orthotopic Xenograft Models for Translational Research

Susan M Irtenkauf, Susan Sobiechowski, Laura A Hasselbach, Kevin K Nelson, Andrea D Transou, Enoch T Carlton, Tom Mikkelsen, and Ana C deCarvalho*

Glioblastoma is an aggressive primary brain tumor predominantly localized to the cerebral cortex. We developed a panel of patient-derived mouse orthotopic xenografts (PDOX) for preclinical drug studies by implanting cancer stem cells (CSC) cultured from fresh surgical specimens intracranially into 8-wk-old female athymic nude mice. Here we optimize the glioblastoma PDOX model by assessing the effect of implantation location on tumor growth, survival, and histologic characteristics. To trace the distribution of intracranial injections, toluidine blue dye was injected at 4 locations with defined mediolateral, anterioposterior, and dorsoventral coordinates within the cerebral cortex. Glioblastoma CSC from 4 patients and a glioblastoma nonstem-cell line were then implanted by using the same coordinates for evaluation of tumor location, growth rate, and morphologic and histologic features. Dye injections into one of the defined locations resulted in dye dissemination throughout the ventricles, whereas tumor cell implantation at the same location resulted in a much higher percentage of small multifocal ventricular tumors than did the other 3 locations tested. Ventricular tumors were associated with a lower tumor growth rate, as measured by in vivo bioluminescence imaging, and decreased survival in 4 of 5 cell lines. In addition, tissue oxygenation, vasculature, and the expression of astrocytic markers were altered in ventricular tumors compared with nonventricular tumors. Based on this information, we identified an optimal implantation location that avoided the ventricles and favored cortical tumor growth. To assess the effects of stress from oral drug administration, mice that underwent daily gavage were compared with stress-positive and -negative control groups. Oral gavage procedures did not significantly affect the survival of the implanted mice or physiologic measurements of stress. Our findings document the importance of optimization of the implantation site for preclinical mouse models of glioblastoma.

Abbreviations: CSC, cancer stem cells; GFAP, glial fibrillary acidic protein; HPA, hypothalamic–pituitary–adrenal; MG, mock gavage; MH, minimally handled; PDOX, patient-derived orthotopic xenograft; PO, predator odor; PP, pseudopalisading; SVZ, subventricular zone

Glioblastoma is the most common and aggressive primary central nervous system malignant tumor in humans.[32] Despite advances in the standard of care, glioblastoma prognosis remains dismal, with a 2-y survival rate of 15.2% for tumors diagnosed between 2008 and 2012 in the United States.[32] Better treatments are urgently needed, and demand research models that accurately represent the heterogeneous genomic characteristics of these tumors. In past decades, glioblastoma cells have been cultured in traditional medium containing 10% FBS. However, glioblastomas have recently been found to contain cells with a stem-cell phenotype,[14] and these tumors can be cultured in serum-free medium originally formulated for the selection and expansion of neural stem cells.[36] This culture condition selects for cells with stem-cell properties, which grow as floating multicellular spheroids, commonly referred to as neurospheres,[8] mimicking the behavior of adult mammalian neural stem cells.[36] Glioblastoma cancer stem cell (CSC) cultures present long-term self-renewing potential, are tumorigenic, present multilineage differentiation potential, and preserve the genotype of the original tumor. In contrast, the cells cultured in 10% FBS are usually not tumorigenic at low passages and diverge considerably from the original tumors at late passages,[24] thus limiting their use as clinically relevant models. Patient-derived CSC cultures are amenable to functional genomics and high-throughput drug screening but do not represent some of the hallmarks of glioblastoma, such as angiogenesis, tissue invasion, and tumor heterogeneity, which are dependent on the natural brain microenvironment. The preclinical development of cancer therapeutics depends on appropriately designed studies using models that recapitulate the molecular diversity and intratumoral heterogeneity of patient tumors.[12] Although response to drugs can be assessed easily in subcutaneous tumor xenografts, important aspects of the disease, such as metastasis in carcinomas and invasion in glioblastomas, are absent.[13] The fact that glioblastomas very rarely grow outside of the brain in humans further underlines the importance of the brain microenvironment in studying key aspects of the disease. Because glioblastoma pathology is better reproduced in the mouse brain than in an ectopic environment, CSC are commonly implanted into immunocompromised mouse brains, for the development of glioblastoma patient-derived orthotopic mouse xenografts (PDOX).[8,11,14,22,24,45]

Received: 22 Jul 2016. Revision requested: 15 Sep 2016. Accepted: 06 Dec 2016.
Hermelin Brain Tumor Center, Department of Neurosurgery, Henry Ford Hospital, Detroit, Michigan.
**Corresponding author. Email: adecarv1@hfhs.org*

For increased translational value of drug studies, glioblastoma PDOX from each patient must develop reproducible tumors that recapitulate the features of the original biopsy. Histologically, glioblastoma is characterized by areas of necrotic tissue, hyperplastic blood vessels, and a high degree of microvascular proliferation. The anatomic distribution for malignant gliomas is predominantly in the frontal, temporal, and parietal lobes of the cerebral cortex, with only 1% to 2% of tumors present in the ventricles.[23,32] In a study involving a large number of patients with newly diagnosed glioblastoma, multifocal tumors were present in only 12% of subjects and were associated with a worse prognosis.[34] Another study classifying glioblastomas according to the anatomic location as determined by MRI identified 4 groups according to subventricular zone (SVZ) and cortex involvement. The SVZ-associated tumors were more likely to present multifocal tumors, rapid progression, and decreased survival.[17,26]

Here we assessed the extent to which the location of intracranial implantation of glioblastoma CSC into mice affects tumor growth rate and pattern, morphology, and histologic characteristics. Dye distribution into brain structures was evaluated immediately after injection of toluidine blue at 4 different intracranial coordinates in nude mice. Next, patient-derived glioblastoma CSC with diverse molecular profiles were implanted by using the same coordinates to assess tumor growth pattern, properties, and symptoms.

In preclinical studies, candidate anticancer drugs are commonly administered to glioblastoma mouse PDOX by oral gavage, requiring brief but firm restraint of alert mice to prevent soft tissue damage, tracheal administration, or aspiration during the procedure and to ensure accurate dosing. Gavage procedures have been shown to elicit increased glucocorticoid production, as well as elevated heart rate and blood pressure for 30 to 60 min,[1] indicating a systemic stress response resulting from activation of the hypothalamic–pituitary–adrenal (HPA) axis.[46] Among other functions, the HPA axis facilitates interaction between the immune and endocrine systems in response to stressors.[7,30] Chronic stress resulting from daily gavage may overstimulate the HPA axis which, in humans, is linked to increased inflammation, angiogenesis, and suppression of the immune response to malignancy.[29] Because stress potentially can lead to undesirable variability in preclinical experiments, we have investigated the potential effect of repeated restraint and oral gavage on tumor growth in the glioblastoma mouse PDOX model. Here we compared the response in nude mice to repeated oral gastric gavage with that of repeated exposure to predator odor, a known stimulus producing an anxiety-like state in naïve rodents.[20] Minimally handled mice served as a negative control for stress. The effects of stress were assessed by measuring changes in body weight, survival, fecal corticosterone levels, and adrenal gland weights.

Our results underscore the importance of optimizing the implantation location for xenograft glioblastoma mouse PDOX models to ensure consistency in tumor growth in appropriate anatomic locations, survival, and histologic characteristics representative of human glioblastoma. The optimization of glioblastoma PDOX models has a direct effect on the translational value of preclinical drug studies.

Materials and Methods

Experimental animals. Nude mice, which lack T lymphocytes but produce natural-killer cells and B cells, have been used as hosts for human xenografts for decades.[37,40] Female nude mice are commonly used in preclinical studies involving brain tumor xenografts, due to their lower aggressiveness relative to that of male nude mice. Less aggressive behavior is preferred in group-housed mice because it reduces the risk of injuries when randomizing or pooling mice; such injuries might represent a confounding factor in the studies. In humans, glioblastoma affects both men and women, and the incidence rate is 1.58 higher in men.[32] A total of 360 female NCRNU-M athymic nude mice (Taconic Farms, Hudson, NY), which were 7 wk old and weighed 17 to 19 g on arrival at our facility, were used in this study (Table 1). Mice were socially housed 5 per cage with enrichment provided on an individually ventilated rack (Alternative Design, Siloam Springs, AR) at the laboratory animal facility of Henry Ford Hospital. Mice were free of all murine pathogens (HM Assessment Plus, Charles River, Wilmington, MA). Environmental enrichment consisted of Shepherd Shacks (Shepherd Specialty Papers, Richmond, MI), Bed-r'Nest (The Andersons Lab Bedding, Maumee, OH), and Aspen Chew Sticks (Lomir Biomedical, Malone, NY). The room was kept on a 12:12-h light:dark cycle, at 22 ± 2 °C, and at 65% ± 2% relative humidity. Mice were provided water and Harlan Teklad (Indianapolis, IN) Laboratory Diets 7012, LM-485 Sterilizable Mouse/Rat Diet without restriction. Cages, bedding, water, water bottles, and all supplies and enrichment devices were sterilized and changed weekly. All personnel having contact with the mice were required to wear a cap, mask, shoe covers, and a sterile gown. Disposable nitrile gloves were sprayed with Clorox Bleach Germicidal Cleaner (Clorox Healthcare, Oakland, CA) immediately prior to contact with mice with excess removed using a sterile towel. Mice were handled in a BSL1 hood that had been cleaned with Clorox Bleach Germicidal Cleaner immediately prior to use. Mice were allowed a 3-d acclimation period before being ear-tagged by using sterilized stainless steel ear tags (National Band and Tag, Newport, KY) with unique 4-digit numbers; after ear-tagging, mice were allowed a 1-wk acclimation period before experiments began. All experiments were conducted in an AAALAC-accredited facility in accordance with the National Research Council's *Guide for the Care and Use of Laboratory Animals*[16] and the Public Health Service Policy on Humane Care and Use of Laboratory Animals.[31] All experiments were conducted under approved Henry Ford Hospital IACUC protocols.

Intracranial dye injection and glioblastoma cell implantation for mouse orthotopic xenografts. Toluidine blue dye or dissociated glioblastoma CSC were implanted by using the free-hand method[33] at subcortical sites: location 1 (L1), location 2 (L2), location 3 (L3), or location 4 (L4; Figure 1 A). All surgical procedures were conducted in a BSL 1 hood within the animal housing room. All mice were anesthetized with ketamine (150 mg/kg) and xylazine (20 mg/kg) by intraperitoneal injection in groups of 10 and returned to a holding cage briefly before being placed on a warm circulating water blanket in sternal recumbency. Artificial Tears (AKORN Animal Health, Lake Forest, IL) was applied to both eyes. The surgical area was scrubbed 3 times, alternating between povidone–iodine and 70% isopropyl alcohol. Surgical anesthesia was confirmed by the loss of pedal reflex. A 5- to 7-mm sagittal incision was made through the scalp to the right of the midline, and the periosteum was retracted by gently scrubbing with a sterile cotton swab soaked in 3% hydrogen peroxide. A small ruler, predrilled to accommodate the 4 implantation locations selected for this study, was aligned with bregma, and a small opening in the

Table 1. Number of mice in each group for the implantation location study

	Implantation location			
	1	2	3	4
Toluidine blue dye	8	4	8	4
GBM1 cells	27	9	9	16
GBM2 cells	7	NA	7	16
GBM3 cells	29	NA	13	43
GBM4 cells	16	NA	NA	20
U251^{fluc} cells	10	NA	NA	8
GBM3^{fluc} cells	14	NA	NA	12

NA, not applicable

skull was manually drilled by using a 25-gauge needle. To serve as a depth guide for the injection needle, a sterile 10-µL pipette tip (Rainin, Oakland, CA), trimmed to the appropriate length for each location, was fitted as a sleeve over a 10-µL Hamilton syringe. The needle was gently inserted into the skull opening and retracted approximately 0.5 mm to accommodate the injection volume. Toluidine blue dye solution (5 µL) or glioblastoma cell suspension (3×10^5 cells in 5µL PBS) was injected slowly over 1 min. Before being gently withdrawn, the syringe was held in place for an additional 30 s to prevent efflux of injected material. Bone wax (Ethicon, Somerville, NJ) was applied to close the skull opening by using a sterile cotton swab, and then the skin was closed with 2 or 3 surgical staples and swabbed with povidone–iodine. Mice were placed in lateral recumbency for recovery in the home cage, with half of the cage placed on a surgical heating pad.

Subjects were monitored for anesthetic recovery and postsurgical pain every 10 min during anesthetic recovery until regaining the ability to maintain an upright posture and walk normally, every 30 min for the following 4 h, and daily thereafter. Diet Gel Recovery (Clear H2O, Westbrook, ME) was provided to each cage immediately after surgery and on days 1 through 3 postsurgically to encourage food and water consumption during initial recovery. No postsurgical changes in behavior or attitude, such as social isolation and reduced activity level, were observed. Mice moved freely with a normal posture, did not appear anxious or aggressive, and continued to eat and drink normally as evidenced by body weight measurements and appropriate hydration. There was no evidence of mice excessively grooming or scratching the incision site or vocalizing. Warmed lactated Ringer solution (2 mL) was administered subcutaneously as needed to maintain hydration during recovery. Mice were weighed 3 times each week—on Monday, Wednesday, and Friday—and were monitored daily for wellbeing assessment, which included hydration status, and signs of pain or distress. In addition, mice were monitored Monday through Friday for signs of tumor growth, including cranial protuberance and neurologic deficits manifested as seizures and abnormal gait or posture. Mice were euthanized by isoflurane overdose prior to decapitation at the completion of the study or at the first signs of neurologic deficit or weight loss greater than 20%.

Dye preparation. Toluidine blue dye (catalog no. 89640, Sigma, St Louis, MO) was dissolved at 0.5 g in 20 mL of 95% ethanol before the addition of 80 mL of distilled water to yield a 0.5% w/v solution. The solution was mixed, filtered through a 0.45-µm syringe filter, and stored at 4 °C protected from light. Dye was filtered a second time through a 0.45-µm syringe filter immediately prior to use.

Glioblastoma cell culture. Resected brain tumors were collected at Henry Ford Hospital (Detroit, MI) with written consent from patients in accordance with institutional guidelines and an approved Institutional Review Board protocol. Tumors were graded pathologically according to the WHO criteria.[27] Glioblastoma specimens were dissociated and cultured in serum-free neurosphere medium to enrich CSC.[5,11] Five glioblastoma CSC lines that grew as neurospheres and that differed in their molecular characteristics were used in this study (GBM1 through GBM5 [Table 2]). For implantation, neurospheres were dissociated to single cells in Dulbecco PBS. In addition, the traditional human glioblastoma cell line U251 (American Type Culture Collection, Manassas, VA) was cultured in media supplemented with 10% FBS and enzymatically dissociated prior to implantation.

Tissue harvesting, histology, immunohistochemistry. A total of 24 mice (Table 1) were injected with toluidine blue dye; they were euthanized 20 min after injection by isoflurane overdose, followed by decapitation. Whole brains were quickly removed and 4 coronal sections (thickness, 2 mm) were obtained using a mouse precision brain slicer matrix (Braintree Scientific, Braintree, MA). Dye dissemination in the unprocessed 2-mm sections was analyzed immediately (Eclipse E800 fitted with a 1× lens, Nikon, Tokyo, Japan).

In addition, 256 mice were implanted with glioblastoma CSC (Table 1) and were euthanized by isoflurane overdose at the completion of the study or at the first signs of neurologic deficit or weight loss greater than 20%. Whole brains were quickly removed, cut into 2-mm coronal blocks as described earlier, and immediately fixed in formalin with subsequent paraffin embedding. Prepared tissue sections 5 µm thick were stained with hematoxylin and eosin to enable visualization of brain structures. Additional GBM3 sections were stained using the Gordon and Sweet stain for reticulin fibers.

For immunohistochemistry, tissue slides underwent 15 min incubation in citric acid buffer pH 6.0 for antigen retrieval, followed by incubation in Rodent Block M (Biocare Medical) for 20 min. The following primary antibodies and dilutions were used: human marker major histocompatibility complex I (MHCI; ab52922, Abcam, Cambridge, UK), 1:1000 for 60 min; endothelial cell marker CD31 (ab28364, Abcam), 1:75 for 60 min; hypoxia marker hypoxia-inducible factor 1α (Hif1α; ab51608, Abcam) 1:250 for 60 min; and astrocytic marker glial fibrillary acidic protein (GFAP; ab33922, Abcam), 1:1200 for 60 min. After primary antibody incubation, slides were incubated for 30 min in Rabbit on Rodent Polymer (Biocare Medical) and for 4 min in Betazoid DAB (Biocare Medical). Images were captured by using a Nikon E800M microscope and DXM1200C digital camera with Image Pro Plus software (Media Cybernetics, Rockville, MD). Stained sections were examined for tumor location and subjectively rated for hallmark glioblastoma histopathology, including blood vessel abnormalities, hypoxia, astrocytic marker staining, necrosis, and thrombosis.

Bioluminescence imaging. A subset of 44 mice implanted with glioblastoma CSC were implanted with cells constitutively expressing firefly luciferase, GBM3^{fluc} and U251^{fluc}, at L1 and L4 (Table 1). Subjects were monitored for tumor progression weekly by using noninvasive bioluminescence imaging (BLI; Xenogen IVIS

A

	Coordinates			Dye distribution
	ML	AP	DV	Ventricular / total
location 1 (L1)	-2.5	0	-3	8/8
location 2 (L2)	-4	0	-3	0/4
location 3 (L3)	-2.5	-1	-2.5	0/8
location 4 (L4)	-2.5	-1	-3	0/4

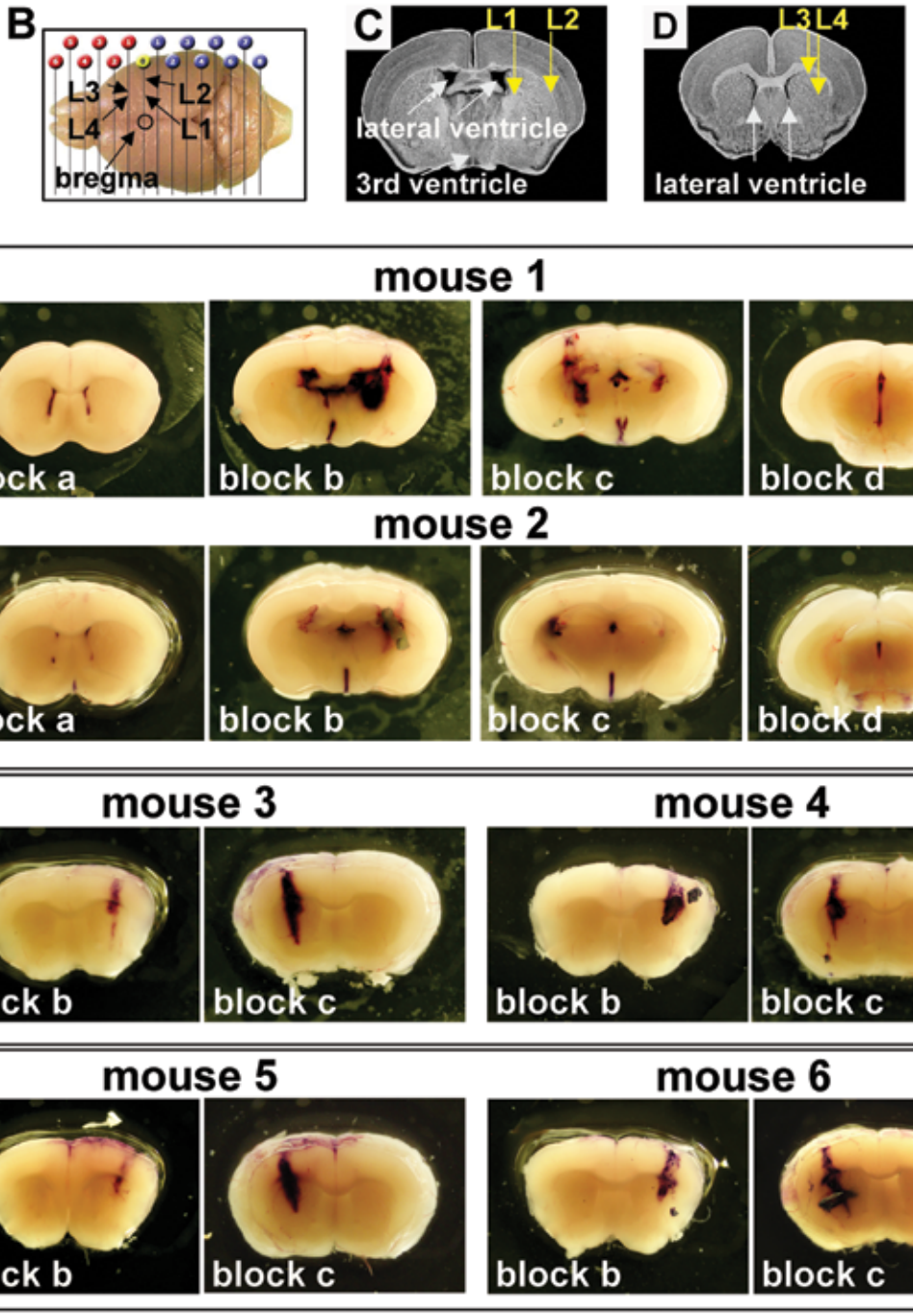

Figure 1. Toluidine blue dye distribution at 4 intracranial implantation locations in nude mice. (A) The 4 locations (L1–L4) for intracranial dye injection are defined by mediolateral (ML), anteroposterior (AP), and dorsoventral (DV) coordinates, relative to bregma. The total number of mice injected and a summary of the dye distribution in the ventricles are shown. (B) The position of the injection sites from a dorsal view of the mouse brain. (C) Positions of L1 and L2 in a coronal brain view. (D) Positions of L3 and L4 in a coronal mouse brain view more anterior to that for panel C. E) Representative images of 2-mm coronal mouse brain blocks a (anterior) through d (posterior), showing the extent of dissemination of toluidine blue dye at 20 min

Table 2. Clinical information associated with the patient-derived cancer stem cells

	Pathology	Treatment status	Tumor location	Age/Sex	MGMT promoter	Time (d) to progression	Overall survival (d)
GBM1	Glioblastoma	untreated	Right temporal	56/female	Methylated	232	360
GBM2	Glioblastoma	untreated	Left temporal	55/female	Methylated	555	664
GBM3	Glioblastoma-variant gliosarcoma	untreated	Left parietal–occipital	62/male	Unmethylated	88	317
GBM4	Glioblastoma	BCNU	Left frontal	61/male	Unmethylated	60	196
GBM5	Glioblastoma	untreated	Right temporal	45/male	Unmethylated	88	646

System, Caliper Life Science, Waltham, MA). Beginning 1 wk after tumor cell implantation, mice were transported in their home cages to the testing room once weekly. The anesthetic induction chamber and imaging chamber were disinfected with Clorox Bleach Germicidal Cleaner and 70% ethyl alcohol, respectively, before use and between groups. Groups of 5 mice were injected with luciferase substrate D-luciferin (150 mg/kg IP) and placed into an isoflurane induction chamber containing 3% isoflurane and 1.5 L/min O_2. Once anesthesia level was confirmed by the loss of pedal reflex, mice were placed into the isoflurane manifold in sternal recumbency within the imaging chamber with 3% isoflurane and 0.3 L/min O_2. Body temperature was maintained during the procedure by using the incorporated warming pad below the anesthetic manifold. BLI began 12 min after substrate injection and continued until peak bioluminescence was recorded, approximately an additional 15 min. Mice were returned to the home cage and monitored for anesthetic recovery. Mice were upright and walking normally within 2 to 3 min and were returned to the housing room.

Stress evaluation and assessment. Female NCRNU-M athymic nude mice (n = 85; age, 8 wk; weight, 17 to 19 g; Taconic Farms, Hudson, NY) were implanted with CSC derived from 2 patients, GBM3 and GBM5, and randomly assigned to 1 of 3 treatment groups (13 to 15 mice per group): mock gavage (MG), predator odor (PO), or minimally handled (MH). PDOX was used here instead of naïve nude mice because tumor burden itself serves as a stressor. The MG group received daily oral gavage with 0.2 mL Ora-Plus (Paddock Laboratories, Minneapolis, MN), a commonly used, orally administered drug vehicle. The PO group, serving as a positive control for stress, was exposed to a cotton ball soaked with 1 mL fox urine (Wildlife Research Center, Ramsey, MN) placed in a ventilated 2-oz. sterile cup for 1 h daily in the home cage with all enrichment devices removed. MG and PO exposures were performed daily for 4 wk beginning 4 wk prior to the time of expected terminal tumor burden for each cell line; this schedule corresponds to the typical drug treatment period used in our preclinical glioblastoma mouse model. Mice in the MG and PO groups were monitored daily for wellbeing assessment and weight collection 3 times each week throughout the duration of the study. On Wednesday of each week, all mice were weighed and immediately placed into clean cages. Enrichment devices were transferred to the new cage and additional clean bedding was added to new cages as needed to replace what had been soiled. At 24 h after the weekly cage change, mice were transferred briefly to a holding cage to allow for collection of feces for subsequent corticosterone analysis. Home cage bedding was sifted through a 12-in. sieve with a 4-mm mesh grid and a collection pan below. All feces produced over the previous 24-h period for each cage was transferred to 50-mL conical tubes and frozen at –80 °C to preserve corticosterone. Sifted bedding and mice were returned to the home cage. MH mice, serving as a negative control for stress, were monitored daily for wellbeing assessment. Body weight measurement and cage changes were performed as described but without the additional 2 weight measurements each week or daily experimental manipulations as for the MG and PO groups. Because cage change is potentially a stressor and might increase corticosterone secretion, the mice were habituated to weekly cage changes from the time of arrival, and all the groups were handled in the same manner during this comparative study. All mice were euthanized by isoflurane overdose at the completion of the study or at the first signs of neurologic deficit or weight loss greater than 20%.

Fecal corticosterone measurements. The steroid hormone corticosterone, which is produced in the adrenal cortex, is the biologically relevant corticosteroid found in mice.[41] To obtain baseline values, feces produced over a 24-h period were collected once each week from each of 3 cages per treatment group for 5 wk, starting 1 wk prior to PO or MG exposure. Feces were collected in 50-mL conical tubes, the weight was measured and normalized by the number of animals in the cage. For corticosterone levels, samples were immediately placed on ice and frozen at –80 °C. Triplicate samples of feces (1.0 g each) from each treatment group were selected randomly, weighed, and dried overnight in a 60 °C oven. Samples were pulverized with a mortar and pestle and corticosterone was extracted in 96% ethanol (0.1 g/mL ethanol) for 40 min at room temperature. Samples were centrifuged at $4200 \times g$ for 15 min at room temperature and ethanol evaporated under vacuum. All samples were stored desiccated at –20 °C until assayed. Fecal corticosterone levels were measured by using a corticosterone ELISA (ENZO, Farmingdale, NY) according to the manufacturer's instructions. Results were calculated in ng/g feces.

Adrenal gland dissection and measurement. Paired adrenal glands were dissected from each mouse and placed in a 60-mm culture dish. Fat and connective tissue were removed under a dissecting microscope. Paired adrenals were blotted dry, weighed, and 2× images captured using a Nikon E800M microscope and DXM1200C digital camera with Image Pro Plus software. Adrenal

after intracranial injection at L1, L3, or L4. In summary, for L1, dye was observed throughout the ventricular system in brain blocks a through d, as exemplified by mice nos. 1 and 2. At L3, dye injections localized exclusively to the injection tract, with no dye observed in the ventricular system (mice nos. 3 and 4). Similar to observations for L3, dye injections at L4 also localized exclusively to the injection tract (mice nos. 5 and 6). Scale bar, 1000 µm (in E but applies to all panels).

gland size (mm^2) was calculated from captured images by using ImageJ.[38] The ratio of the paired adrenal gland weight to peak body weight was calculated by using the highest body weight for each mouse immediately prior to the decline due to tumor burden.

Statistical analysis. Statistical analyses were performed using GraphPad Prism 6 (GraphPad Software, La Jolla, CA). Observers were blinded to the experimental groups, where possible. Unpaired *t* tests or one-way ANOVA, followed by *t* tests for individual group comparisons, were used as described for each experiment. Fisher exact tests were used to compare incidence of ventricular tumors in different implantation locations. Kaplan–Meier survival curves were compared by using the log-rank Mantel–Cox test. Unpaired *t*-tests were used to compare the observed histologic characteristics of ventricular and nonventricular tumors. For all comparisons, a *P* value of less than 0.05 was considered significant.

Results

Testing intracranial implantation coordinates with tracer dye. Preclinical research requires that patient-derived mouse xenografts present consistent, reproducible intracranial tumor growth and symptom development. Human glioblastoma tumors are located predominantly within the cerebral cortex and infiltrate the brain parenchyma. Because the mouse cortex proportionally comprises a smaller fraction of the brain, to favor tumor growth into the cortex and to prevent cell efflux through the craniotomy and subsequent superficial tumor growth, tumor cells were implanted into subcortical locations in mice.[3,33] To trace the distribution of the contents of intracranial injections, 5 µL of toluidine blue dye solution was injected into 4 to 8 animals per group (Table 1) at 4 distinct sets of coordinates (Figure 1 A through D) and by using the same protocol as for tumor cell implantation. Mice were euthanized 20 min after dye injection, whole brains were removed, and 4 coronal tissue blocks (2-mm thickness) were obtained and labeled from anterior to posterior (a through d). Tissue blocks were examined immediately under a microscope to evaluate the dissemination of dye into surrounding brain structures, and images were captured (Figure 1 E). According to a published atlas,[35] dye injected at L1 (ML, –2.5; AP, 0; DV, –3.0) was expected to be localized to the central striatum, ventral to the corpus callosum. Coordinates in the atlas are based on adult (26 to 30 g) C57BL/J6 mice, whereas smaller (17 to 19 g) and younger (5 to 8 wk) nude mice are typically used for patient-derived models. Indeed in the 8-wk old- female nude mice used in this study, the injection tract and dye distribution were more posterior than expected and lay immediately adjacent to the lateral ventricle (Figure 1 C). Intraventricular dye dissemination was observed in all 8 mice injected at L1 (Figure 1 A and E). Dye injected at L2 (ML, –4.0; AP, 0; DV, –3.0), which was 1.5 mm lateral relative to L1 (Figure 1 B and C), resulted in dye localization to or immediately adjacent to the injection tract in all 4 subjects tested (Figure 1 A). However, injections at this location were difficult to execute due to the extreme lateral placement of the injection. Needle insertion was compromised by the proximity to the bony ridge at the edge of the parietal bone. L3 dye injections (ML, –2.5; AP: –1; DV: –2.5), 1 mm anterior to L1 (Figure 1 B and D) similarly resulted in dye at or immediately adjacent to the injection tract in all 8 subjects, with no evidence of ventricular dye dissemination (Figure 1 A and E). Similar to that for injection at L3, dye localization at L4 (ML, –2.5; AP, –1; DV, –3.0) was at or immediately adjacent to the injection tract in all 4 subjects, with no evidence of ventricular dye dissemination (Figure 1 A and E). L4 injections were placed 0.5 mm deeper than L3 injections (Figure 1 B and D) to provide a deeper pocket for the injected volume, thus minimizing the risk of efflux.

Effect of implantation site on anatomic location of tumor growth. After tracking the dissemination of dye at 4 implantation locations, we assessed the effect of glioblastoma CSC implantation at the same locations on tumor growth rate, pattern, and morphologic characteristics. Glioblastoma patient-derived CSC lines GBM1, GBM2, GBM3, and GBM4 were selected to represent diverse clinical and molecular characteristics (Table 2), and one nonstem serum-cultured cell line, $U251^{fluc}$, was included in the study for comparison (Table 1). For drug studies, typically large cohorts of mice are implanted with the same batch of tumor cell suspension and randomized to several treatment arms to ensure uniformity of initial tumor cell inoculation. Single-cell suspensions (3×10^5 viable cells per mouse) were implanted at L1, L2, L3, or L4 (Figure 1 A through D). Mice were euthanized by isoflurane over Glioblastoma patient-derived CSC lines dose followed by decapitation at the completion of the study or at the first signs of neurologic deficit or weight loss greater than 20%. Tumor location was assessed histologically in coronal brain sections stained with hematoxylin and eosin and labeled with an antibody to the human marker MHCI.

Results for GBM1 cells were consistent with dye distribution results (Figure 1 A and E). Nonventricular tumors (Figure 2 A, left column) were localized to the subcortical and cortical regions, presenting necrosis and thrombosis, further described below. Human glioblastoma is characterized by areas of necrosis surrounded by infiltrative tumor cells.[27] Ventricular tumors by contrast were small, obstructive, multifocal, and without necrosis or infiltrating tumor cells (Figure 2 A, right column). Ventricular tumors were observed in 16 of 27 (59.26%) subjects implanted at L1 (Figure 2 B). In contrast, significantly fewer subjects implanted at L4 had ventricular tumors, 2 of 16 (12.5%; Figure 2 B; Fisher exact test, $P < 0.0038$). Ventricular tumor growth was not observed in subjects implanted at L2 (0 of 9; Figure 2 B; Fisher exact test, $P = 0.0019$). These tumors were localized to the extreme lateral cortex with very diffuse tumor in subcortical areas. Consistency of tumor cell implantation at this location was predicted to be very difficult due to the extreme lateral placement, as described above. Similar to L4 implants, L3 implants resulted in tumors extending from the subcortical regions into the cortex, with ventricular tumors occurring in only 1 of 9 (11.1%) subjects (Figure 2 B; Fisher exact test, $P = 0.0198$).

Glioblastoma is characterized by both marked intertumor and intratumor heterogeneity, challenging the development of novel therapies.[15] We have developed a mouse PDOX panel to study the heterogeneity of glioblastoma observed across the patient population and to move toward a personalized approach to patient therapy.[4,5,11] To assess to what extent tumor heterogeneity and differential growth characteristics would affect these results, additional glioblastoma cell lines were examined under the same conditions. GBM2 cells were implanted at L1, L3, and L4. Ventricular tumors were present in 5 of 7 (71.43%) subjects implanted at L1 (Figure 2 B). Significantly fewer ventricle tumors, 1 of 16 (6.25%), were observed in subjects implanted at L4 (Figure 2 B; Fisher exact test, $P = 0.0034$). Similarly, no ventricular tumors were observed for subjects implanted at L3 (Figure 2 B; Fisher

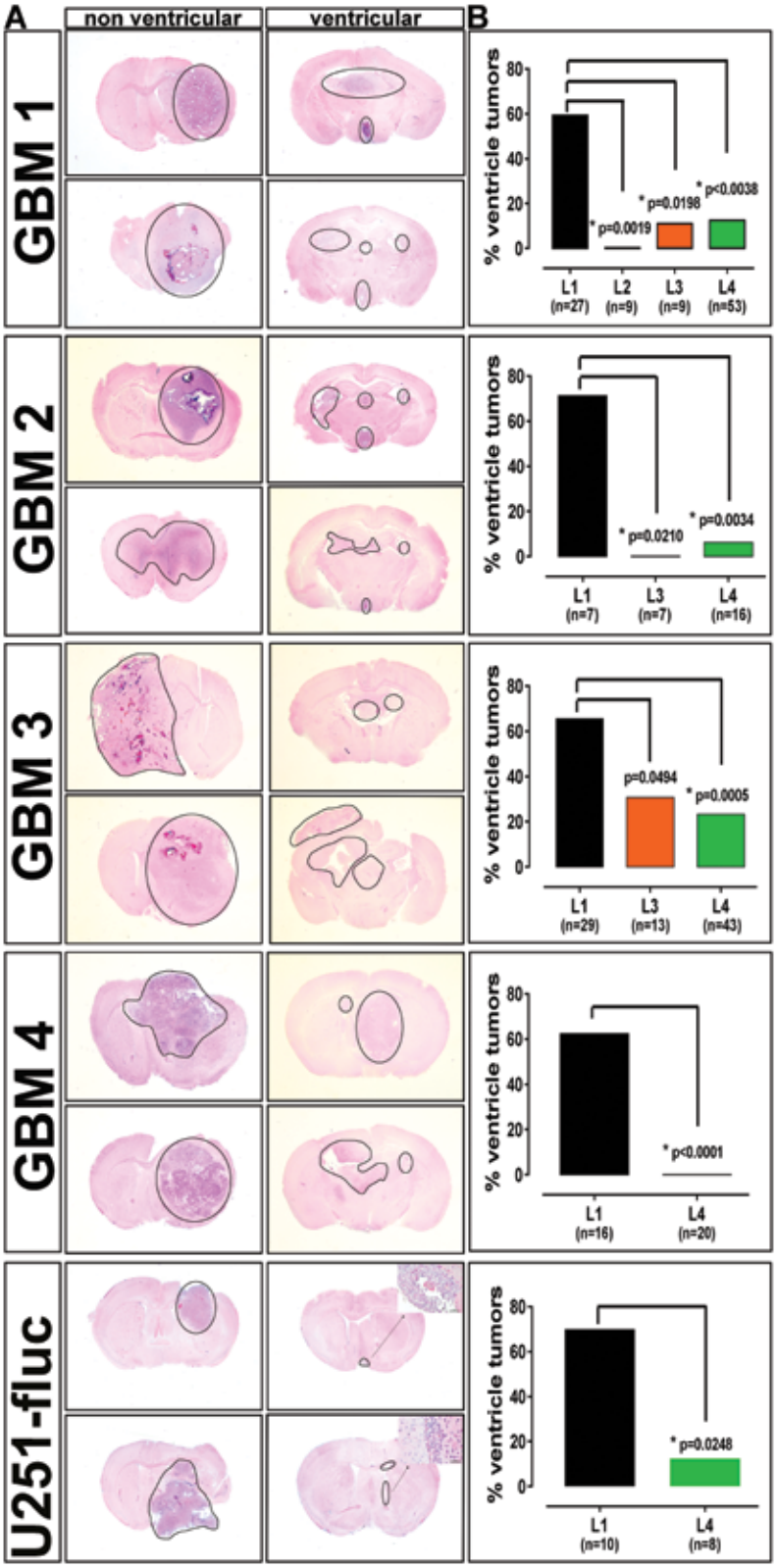

Figure 2. Tumor growth pattern and frequency of ventricular tumors in glioblastoma patient-derived orthotopic xenografts from different implantation sites. (A) Representative images of coronal brain sections from mice implanted intracranially with 4 patient-derived glioblastoma CSC (GBM1 through GBM4) and a traditional glioblastoma cell line (U251^{fluc}), exemplifying nonventricular (left column) and ventricular (right column) tumor localization for each model. Tumors that localized to the subcortical and cortical regions were large, well-vascularized and necrotic, thus recapitulating human glioblastoma, whereas tumors that localized to the ventricular system were typically small and multifocal and lacked a central necrotic core. Hematoxylin

exact test, $P = 0.0210$). We observed a higher frequency of tumors growing at the outer surface of the cortex for GBM2 implanted at L3 (data not shown) but not for other cell lines, possibly due to increased efflux at the more superficial injection site. Consequently, the increased depth of L4 was better suited to contain the injection volume and minimize superficial tumor growth for the CSC lines that present this propensity.

Results for GBM3 implanted subjects were similar, with ventricular tumors present in 19 of 29 (65.52%) subjects implanted at L1 (Figure 2 B). Significantly fewer ventricular tumors were observed in subjects implanted at L4, 10 of 43 (23.26%) subjects (Figure 2 B; Fisher exact test, $P = 0.0005$). Again, as a consequence of the differential growth characteristics of these cell lines, some ventricular tumors extended into the surrounding subcortical and cortical regions, although this growth was more diffuse with no central necrotic core, as is typically seen both in human glioblastoma and in nonventricular xenograft tumors in our models (Figure 2 A). Ventricular tumors were observed in 4 of 13 (30.77%) of subjects implanted at L3, significantly fewer than occurred at L1 (Figure 2 B; Fisher exact test, $P = 0.0494$). Due to the technical difficulties associated with the extreme lateral location of L2, and increased efflux of cell suspension for some lines at L3, as described earlier, GBM4 was implanted at L1 and L4 only. Ventricular tumors were observed in 10 of 16 or 62.5% of L1 subjects, whereas none of the 20 L4 subjects had intraventricular tumors (Figure 2 B; Fisher exact test, $P < 0.0001$). Similar to GBM3, some GBM4 ventricular tumors infiltrated diffusely into the surrounding subcortical and cortical regions (Figure 2 A). Mice with multifocal ventricular tumor growth presented tumor burden symptoms in the absence of significant tumor mass in the subcortical and cortical regions, possibly suggesting obstructive hydrocephalus.

These results indicate that the brain coordinates used for CSC implantation significantly affect xenograft tumor localization and growth patterns. CSC are propagated in selective serum-free media and retain the ability to self-renew and differentiate after implantation, whereas nonstem glioblastoma cells grown in media containing serum for many passages undergo irreversible differentiation.[24] To test to what extent implantation location might affect tumor localization of a traditional serum-cultured nonstem glioblastoma cell line, we implanted U251^{fluc} cells, modified to constitutively express firefly luciferase, at L1 and L4. As seen with CSC lines, implantation at L1 resulted in significantly higher frequency of ventricular tumors, 7 of 10 (70%) subjects, compared with 1 of 8 (12.5%) subjects implanted at L4 (Figure 2 B; Fisher exact test, $P = 0.0248$). Despite presenting weight loss greater than 20% and significant neurologic symptoms at the time of euthanasia, only small clusters of tumor cells attached to the ventricle walls occurred in most of the U251^{fluc} subjects in the L1 group (Figure 1 A). Nonventricular tumors observed in most L4 subjects were large and extended from the subcortical areas into the cortex (Figure 2 A). These results indicate that the effect of implantation location on glioblastoma tumor growth patterns is not restricted to CSC.

Despite the nonuniform characteristics intrinsic to these glioblastoma models, the data in Figure 2 B show that for each of the 5 lines, the implantation location L1 resulted in 60% to 70% incidence of ventricular tumors compared with 0% to 23% at L4. These results indicate that ventricular growth is significantly affected by implantation location in all 5 models. The ventricular tumor incidence for L4 varied among the lines, from 0% for GBM4 to 23% for GBM3.

Comparison of ventricular and nonventricular tumors in regard to mouse survival and tumor growth rate. We have established above that implantation location significantly affects to what extent intracranially injected tumor cells become established and produce tumors in the mouse ventricle or striatum and cortex. We next evaluated the clinical relevance of ventricular and nonventricular tumors in terms of tumor growth rate, survival, histopathology, and morphologic characteristics.

All subjects were euthanized when symptoms of terminal tumor burden—such as greater than 20% weight loss, hunched posture, cranial protrusion, and significant neurologic symptoms—were observed. For GBM1 PDOX, the median survival for mice with ventricular tumors was 34 d compared with 39 d for those with nonventricular tumors (Figure 3 A; log-rank test, $P = 0.0143$). Median survival for GBM2 PDOX was significantly reduced for subjects with ventricular tumors compared with nonventricular tumors, 21.5 and 33.5 d, respectively (Figure 3 B; log-rank test, $P = 0.0034$). Survival for mice implanted with GBM3 presenting ventricular compared with nonventricular tumors was 74 and 78 d, respectively, which were not significantly different (Figure 3 C; log-rank test, $P = 0.1117$). As described earlier, some GBM3 ventricular tumors infiltrated into the surrounding subcortical areas and cortex, with tumor cells lining the ventricles without obstruction, and this presentation might have minimized the effect on survival that was observed for the other cell lines. Median survival for GBM4 subjects with ventricular tumors was 70 d compared with 79.5 d for subjects with nonventricular tumors (Figure 3 D; log-rank test, $P < 0.0001$). Tumor location likewise affected the survival of the traditional U251^{fluc} xenografts. Median survival for subjects with ventricular tumors was 18 d compared with 34 d for mice with nonventricular tumors (Figure 3 E; log-rank test, $P = 0.0001$). The decreased survival for mice with ventricular tumors is consistent with shorter survival times related to obstructive hydrocephalus caused by ventricular tumors in humans.[21,25,39]

Longitudinal tumor growth was monitored using noninvasive BLI. Cells expressing firefly luciferase (GBM3^{fluc} and U251^{fluc}) were implanted intracranially as described. Once each week, mice were injected intraperitoneally with D-luciferin substrate, and tumor bioluminescence was measured. Although no difference in survival was observed for GBM3 (Figure 3 C), a trend of reduced growth rate was present in subjects with ventricular tumors in the later, rapid growth phase compared with subjects with nonventricular tumors (Figure 3 F), suggesting a decreased tumor burden for ventricular tumors at the time of euthanasia. A comparison of the absolute BLI radiance (p/s/cm^2/sr) showed no difference between GBM3 ventricular and nonventricular tumors at the first measurement at 7 d after implantation (t test, $P = 0.336$) but a significantly higher radiance for nonventricular tumors at the last measurement prior to euthanasia (between 49 and 98 d after implantation; t test, $P = 0.0189$; Figure 3 G). The

and eosin stain; tumor regions are circumscribed; bar, 1000 µm (main images); 50 µm (insets). (B) The incidence of ventricular tumors among the mice according to implantation location for the indicated number of mice. For all mouse models, a higher percentage of ventricular tumors resulted from implants at L1 relative to the other locations; differences were considered significant (*) at $P < 0.05$ (Fisher exact test).

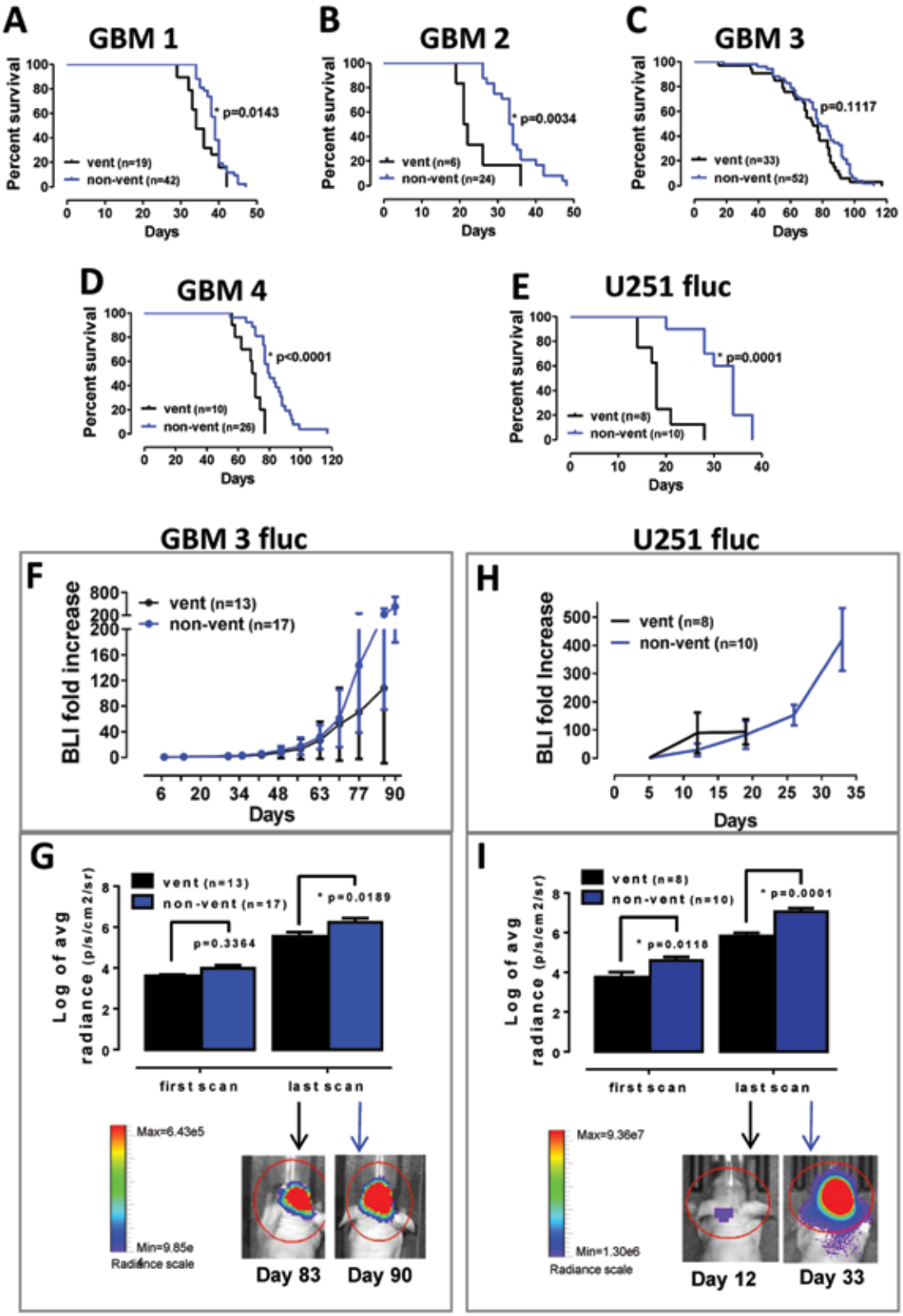

Figure 3. The presence of ventricular tumors influences xenograft tumor growth rate and mouse survival. Comparison of Kaplan–Meier survival curves between the indicated number of subjects with ventricular (vent) and nonventricular (non-vent) tumors by log-rank test for PDOX (A) GBM1 ($P = 0.0143$), (B) GBM2 ($P = 0.0034$), (C) GBM3 ($P = 0.1117$), (D) GBM4 ($P < 0.0001$), and (E) the nonstem-cell line U251^{fluc} ($P = 0.0001$). (F) Results of weekly noninvasive in vivo bioluminescence imaging (BLI) are expressed as fold increase relative to the first measurement in GBM3^{fluc} mice with ventricular or nonventricular tumors. (G) Bioluminescence radiance values (Log2) for ventricular and nonventricular tumors at the first (day 7 after implantation)

BLI fold-increase rate for the nonstem-cell line U251^{fluc} was not affected by the presence of ventricular tumors, possibly due to the significantly shorter survival of these subjects, which were euthanized due to terminal tumor symptoms before the beginning of the rapid growth phase, thus allowing for just 3 measurements (Figure 3 H). In fact, the absolute radiance measurements in the first scan, just 5 d after implantation, were significantly (*t* test, $P = 0.0118$) lower for subjects with ventricular tumors. The difference in absolute radiance increased at the last measurement (between 12 and 33 d after implantation; *t* test, $P = 0.0001$; Figure 3 I). The lower initial BLI measurements for U251^{fluc} ventricular tumors indicate that, for this fast growing xenograft tumor model, the difference in tumor growth dynamics between ventricular and nonventricular tumors can be detected just after implantation.

Histopathology and morphologic characteristics. In addition to growing in the appropriate anatomic location, leading to consistency in survival, another requisite qualifying glioblastoma xenograft models for use in preclinical therapeutic development is recapitulation of the histopathology and morphologic characteristics of human tumors. Images in Figure 2 A indicate histologic differences between ventricular and nonventricular tumors. Next we characterized ventricular and nonventricular terminal tumors in the PDOX tissue relative to typical characteristics of glioblastoma.

Glioblastomas are grade IV astrocytomas, typically expressing the astrocytic marker GFAP. GBM3 is classified as a gliosarcoma, a rare morphologic variant of glioblastoma characterized by biphasic glial and sarcomatous compartments.[28] The glial portion is identified by the expression of GFAP, and the sarcomatous compartment is composed of GFAP-negative, reticulin-positive cells. Nonventricular tumors reproduced the gliosarcoma phenotype with GFAP-positive glial (Figure 4 A) and reticulin-positive sarcomatous (Figure 4 B) compartments. By contrast, ventricular tumors display only the glial GFAP positive compartment (Figure 4 C) and were reticulin negative (Figure 4 D), suggesting that the sarcomatous component of GBM3 might be suppressed in ventricular tumors. GBM4 is a typical glioblastoma, presenting a GFAP-positive nonventricular tumor mass (Figure 4 E) and fewer GFAP-positive cells in ventricular tumors (Figure 4 G). GFAP typically is not expressed in neurospheres in culture but is upregulated after implantation of the mouse xenograft tumors.[5] Adjacent sections of GBM4 (Figure 4 F and H) stained with the human marker MHCI clearly show human tumor cells throughout the area examined for GFAP staining, demonstrating that these tumor cells are indeed negative for GFAP.

Glioblastoma tumors are characterized by dysfunctional and enlarged blood vessels.[18] GBM3 PDOX sections stained with CD31, an endothelial cell marker, indicates that nonventricular tumors have a high degree of hyperplastic blood vessels (Figure 4 I), whereas ventricular tumors were minimally vascularized (Figure 4 J). As for GBM3, GBM2 nonventricular tumors demonstrated more hyperplastic blood vessels (Figure 4 M) than did ventricular tumors (Figure 4 N). For translation of preclinical studies of drugs targeting neoplastic cells or angiogenesis into the clinic, it is important that the hyperplastic blood vessels, a hallmark of glioblastomas, are represented in the PDOX models. Areas of hypoxia (a driver of angiogenesis), abnormal vasculature, and resistance to treatment, are characteristic of glioblastomas.[47] HIF1α, a subunit of the heterodimeric HIF1 transcription factor that regulates O_2 homeostasis, is upregulated in response to hypoxia. HIF1α is upregulated in GBM3 nonventricular tumors, consistent with the prominent vascular hyperplasia observed (Figure 4 K) and, to a lesser degree, in GBM2 nonventricular tumors (Figure 4 O). Less HIF1α expression was noted for GBM3 ventricular tumors (Figure 4 L), whereas GBM2 ventricular tumors presented foci with increased HIF1α expression (Figure 4 P). The data show that the ventricular tumors are small, less vascularized, and present variable levels of hypoxia.

Typical glioblastoma morphologic characteristics were evaluated for ventricular and nonventricular tumors in PDOX. In addition to the abnormal vasculature described earlier, hypercellularity, thrombosis, and necrosis with and without pseudopalisades (PP), which are accumulations of tumor cells around central necrosis, are defining characteristics of human glioblastoma.[27] These characteristics were scored using a 1 to 4 scale from histologic images for terminal tumors of multiple subjects from each PDOX line. Results are summarized in Table 3, and representative images for GBM3 are shown (Figure 4 Q through V). Intratumoral hypercellularity was not affected by ventricular or nonventricular growth, except for a modest increase for nonventricular GBM2 tumors (Table 3). Significantly increased frequency of thrombosis (Figure 4 Q and R), PP necrosis (Figure 4 S and T), and necrosis (Figure 4 U and V) was observed for nonventricular tumors for half of the PDOX lines (Table 3). Ventricular tumors from all glioblastoma PDOX in this study were less invasive compared with nonventricular tumors, with significantly lower frequency of tumor growth in subcortical, cortical and white matter regions (Table 3). Nonventricular tumors invaded the brain parenchyma well beyond the injection tract and into the white matter and contralateral hemisphere (Table 3 and Figure 2 A). Although many of the ventricular tumors for GBM1 and GBM2 were small and multifocal with little invasion into surrounding tissue or white matter, some GBM3 and GBM4 ventricular tumors also infiltrated into the surrounding subcortical and cortical regions (Table 3 and Figure 2 A). However, as mentioned earlier, these infiltrating ventricular tumors exhibited less necrosis and thrombosis than nonventricular lesions. These results show that in a diverse glioblastoma PDOX panel, glioblastoma histopathologic features are indeed better reproduced in tumors without ventricular involvement. We conclude that implantation location and the resulting tumor distribution are critical factors in producing consistent and reproducible mouse orthotopic xenografts that are representative of human glioblastoma.

Stress measurement and effect on PDOX tumor burden. In addition to improving the reliability of tumor formation in our mouse model of human glioblastoma, we examined the effect of stress due to restraint and orogastric gavage on mouse PDOX models. Next we studied whether daily gavage or exposure to predator odor influence tumor growth, survival, adrenal gland weight, body weight, and fecal corticosterone levels in PDOX models. GBM3 and GBM5 PDOX, from 2 newly diagnosed untreated glio-

and last scans for GBM3. (H) BLI fold increase for U251^{fluc} xenografts. (I) Bioluminescence radiance values (log2) for ventricular and nonventricular tumors at the first (day 7 after implantation) and last scans for U251^{fluc}. For panels G through I, the final scans shown are from representative mice in each group, and $P < 0.05$ was considered to define statistical significance (*).

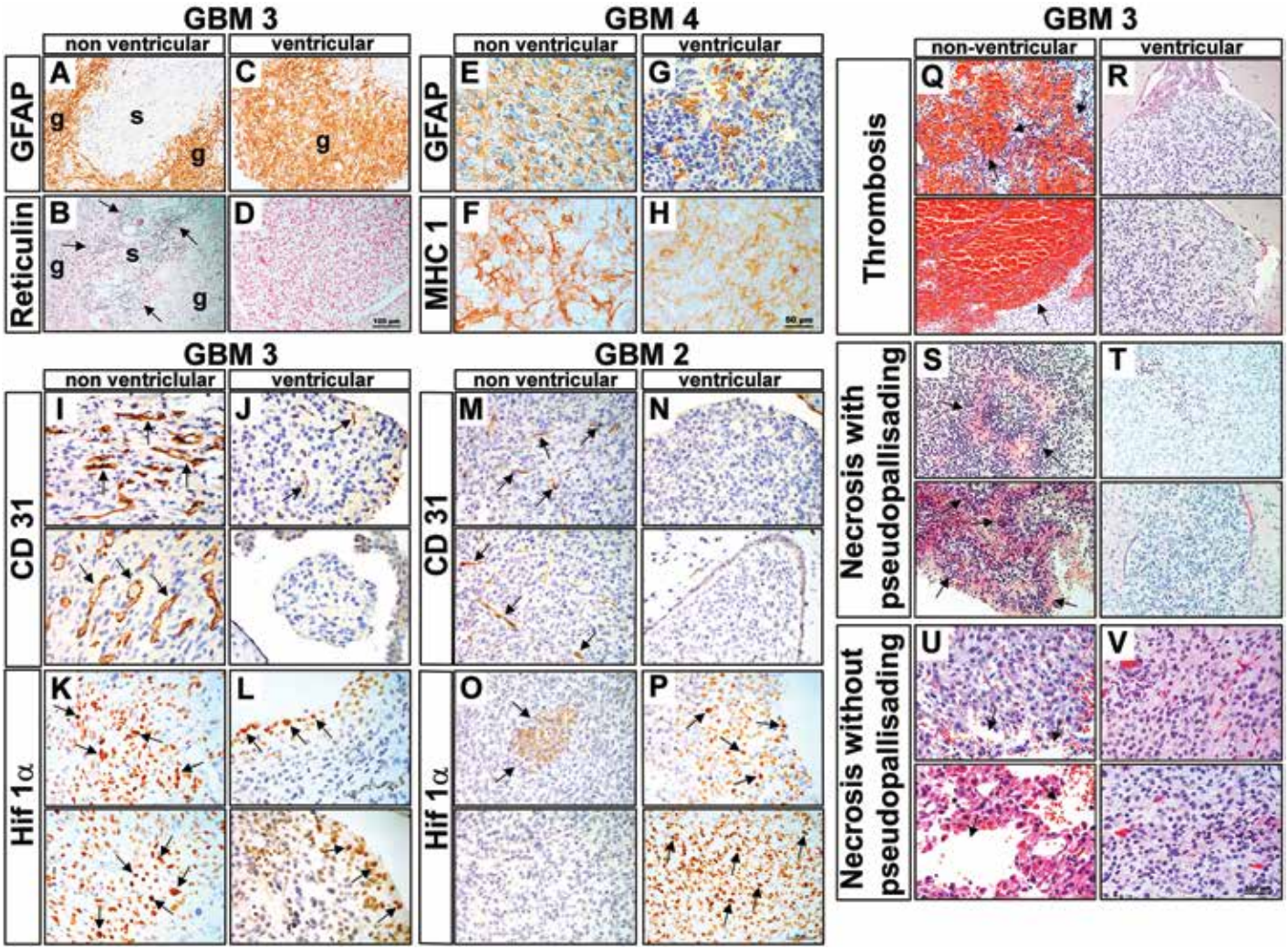

Figure 4. Morphologic features and immunohistologic markers are distinct between ventricular and nonventricular xenograft tumors. (A) GFAP expression and (B) reticulin staining (arrows; adjacent section) in GBM3 PDOX show the biphasic glial (g) and sarcomatous (s) components that characterize the glioblastoma-variant gliosarcoma. The gliosarcoma biphasic staining pattern is suppressed in ventricular tumors, as demonstrated by (C) the loss of GFAP-negative regions and an absence of reticulin staining, thus indicating that (D) only the glial (g) component is present. (E) GFAP is highly expressed in GBM4 nonventricular tumors. (F) An adjacent tissue section is stained with the human marker MHCI. (G) GFAP expression is restricted to cell clusters in the ventricular tumor. MHCI staining reveals human tumor cells throughout the GFAP-negative regions in the adjacent section, indicating that the absence of GFAP staining is not due to a lack of human tumor cells (H). (I) CD31 staining of GBM3 tumors reveals numerous hyperplastic blood vessels (arrows) in nonventricular tumors, typical of human glioblastoma. In comparison, (J) ventricular tumors display much less vascular hyperplasia, particularly in the small spheroid-like tumor masses floating freely in the ventricle. (K) The Hif1α–positive cells in GBM3 indicate greater hypoxia in nonventricular tumors; (L) ventricular tumors were less hypoxic. As for GBM3 tumors, CD31 staining of GBM2 revealed more vascular hyperplasia in (M) nonventricular tumors relative to (N) ventricular tumors. (O) Focal Hif1α-positive cells were observed in GBM2 tumors (arrows) and (P) a larger area of Hif1α-positive cells (arrows) in ventricular tumors. (Q–V) GBM3. Thrombosis was (Q) frequent (arrows) in nonventricular tumors but was (R) absent from ventricular tumors. PP necrosis was (S) prominent (arrows) in nonventricular tumors but (T) absent in ventricular tumors. Similarly, necrosis without pseudopalisades was (U) frequent (arrows) in nonventricular tumors but (V) absent in nonventricular tumor. Scale bars: D, 100 µm (applies to A–D); H, 50 µm (applies to E–P); and V, 100 µm (applies to Q–V).

blastoma patients with unmethylated MGMT promoters (Table 2) and different survival times, were chosen for the stress experiments. Female athymic nude mice were implanted with GBM3 and GBM5 CSC and randomized to MG, PO positive-control, or MH negative-control groups. PO exposure and MG treatment began 4 wk prior to the time of expected terminal tumor burden, which was 6 wk after implantation for GBM3 and 2 wk for GBM5, and lasted for 4 wk, a typical preclinical drug treatment schedule. Mice subjected to chronic stress due to either restraint or social isolation have increased tumor burden and more invasive tumor growth in a mouse model of ovarian cancer.[43] In the current study, there was no significant effect of PO or MG exposure on overall survival compared with the MH groups for either GBM3 (log-rank test, $P = 0.3016$ and 0.2755, respectively; Figure 5 A) or GBM5 (log-rank test, $P = 0.5684$ and 0.7483, respectively; Figure 5 B). Previous studies have shown that body weight measurements of mice exposed to daily restraint-associated stress decrease rapidly and remain lower compared with nonstressed controls, despite

Table 3. Histologic characteristics of PDOX tumors

	Hypercellularity	PP necrosis	Necrosis without PP	Thrombosis	Tumor location		
					Subcortical	Cortical	White matter
GBM1							
Ventricular (n = 5)	2.8 ± 0.60	1.20 ± 1.09	0.90 ± 0.98	0.85 ± 0.89	0.95 ± 0.98	1.15 ± 0.82	2.20 ± 1.02
Nonventricular (n = 10)	3.20 ± 0.33	1.73 ± 1.00	2.41 ± 1.06	2.43 ± 1.46	3.25 ± 1.14	2.98 ± 1.02	2.72 ± 0.86
P	0.1983	0.5388	0.0726	0.0193[a]	0.0073[a]	0.0142[a]	0.4898
GBM2							
Ventricular (n = 6)	3.38 ± 0.14	0.42 ± 0.38	0.25 ± 0.61	0.17 ± 0.30	1.08 ± 1.02	0.38 ± 0.70	1.25 ± 0.71
Nonventricular (n = 10)	3.65 ± 0.13	0.98 ± 0.71	1.03 ± 1.43	1.25 ± 1.24	3.93 ± 0.12	3.2 ± 0.69	2.95 ± 0.71
P	0.0083[a]	0.1036	0.0031[a]	0.0140	0.0006[b]	0.0002[b]	0.0023[a]
GBM3							
Ventricular (n = 9)	2.03 ± 1.53	0.03 ± 0.08	0.17 ± 0.50	0.47 ± 0.90	0.44 ± 0.67	0.14 ± 0.33	0.59 ± 0.76
Nonventricular (n = 5)	3.22 ± 1.4	1.9 ± 1.31	1.42 ± 0.94	2.9 ± 0.72	3.31 ± 0.43	3.14 ± 0.67	2.31 ± 0.91
P	0.0879	0.0008[b]	0.0306[a]	0.0064[a]	<0.0001[c]	<0.0001[c]	0.0024[a]
GBM4							
Ventricular (n = 4)	3.25 ± 0.01	0.0 0 ± 0.00	1.81 ± 1.38	0.50 ± 1.00	0.63 ± 0.95	0.38 ± 0.75	0.50 ± 1.00
Nonventricular (n = 6)	3.50 ± 0.22	2.21 ± 1.20	2.21 ± 0.75	0.79 ± 0.93	3.75 ± 0.50	2.79 ± 1.59	3.21 ± 0.76
P	0.0892	0.0069[a]	0.5678	0.6489	0.0004[b]	0.0012[a]	0.0012[a]

PP, pseudopalisading
Data are given as mean ± 1 SD.
[a]$P < 0.05$ (Unpaired t test)
[b]$P < 0.001$ (Unpaired t test)
[c]$P < 0.0001$ (Unpaired t test)

recovery of food intake.[19] No significant effect of handling stress on mean body weights for each treatment group was observed for GBM3 (Figure 5 A) or GBM5 (Figure 5 B) mice. In addition, body weight change (relative to the last pretreatment measurement) in individual mice after 1 wk of treatment was not significantly different among the treatment groups for either line (1-way ANOVA); Figure 5 A and B). Body weight decline and symptom onset coincided for all groups, suggesting no significant effect on late-stage rapid tumor growth and no effect on symptom-free survival for GBM3 or GBM5 (Figure 5 A and B).

A widely used noninvasive means of assessing response to stressors, fecal corticosteroid measurement was used in the current study in place of plasma corticosterone to avoid the confounding effect of a stress response due to repeated blood sampling.[44] After mice had been treated for 1 wk, their feces were collected over a 24-h period. Fecal corticosterone levels were determined by ELISA and normalized to values from age-matched naïve nude mice samples, which ranged from 1.7 to 6.2 ng corticosterone per gram of feces. There was no significant difference between naïve and tumor-bearing untreated (that is, MH) mice (Figure 5 C). The 24-h fecal excretion of corticosterone was not increased by MG treatment or PO exposure relative to the MH group for GBM3 or GBM5 PDOX (Figure 5 C).

Furthermore, chronic stress has been shown to affect adrenal glands, resulting in increased adrenal weights coinciding with decreased body weights.[6] Here, we investigated the ratio of paired adrenal gland weight to peak body weight, calculated by using the highest body weight for each mouse immediately prior to decline due to tumor burden. Adrenal glands were collected at the time of euthanasia due to terminal tumor burden and the weight normalized to the peak body weight achieved during the course of the experiment. No significant difference in normalized adrenal gland weight was noted for GBM3 or GBM5 (Figure 5 D). Taken together, the data suggest that PO and MG exposure did not significantly alter the physiologic measures of stress or PDOX tumor growth.

Discussion

Patient-derived mouse orthotopic xenografts have great potential for glioblastoma preclinical drug development, due to a better preservation of the diverse genomic and molecular heterogeneity found in the clinical setting,[8,11,14,22,24,45] even recapitulating phenotypes defining rare glioblastoma variants.[5] Human glioblastoma typically presents as a frontotemporal lesion in the cerebral cortex, with only 1% presenting as ventricular tumors.[32] Here we show that implanted CSC that form tumors extending from the subcortical areas into the cortex are more similar to clinical glioblastomas, compared with tumor cells dispersed throughout the ventricular system. We show that glioblastoma PDOX with ventricular tumors have a shorter time to onset of symptoms and shorter overall survival. These mice presented with symptoms similar to those of terminal tumor burden, such as cranial protrusion, sluggishness, gait disturbances, and seizures, thus meeting the criteria for termination, but are found on histologic evaluation to have small and frequently multifocal tumors, resulting in considerable challenges regarding efficient tissue harvest for molecular analysis, an intrinsic component of translational research. Furthermore, the ventricular microenvironment is different from the subcortical areas and cortex, resulting in differences not only in tumor growth rates but also in vasculature, morphology, and immunohistochemical markers, rendering them less representative of the human glioblastoma tumor phenotype.

In humans, glioblastoma typically presents as invasive cortical lesions characterized by necrosis, thrombosis, and abnormal

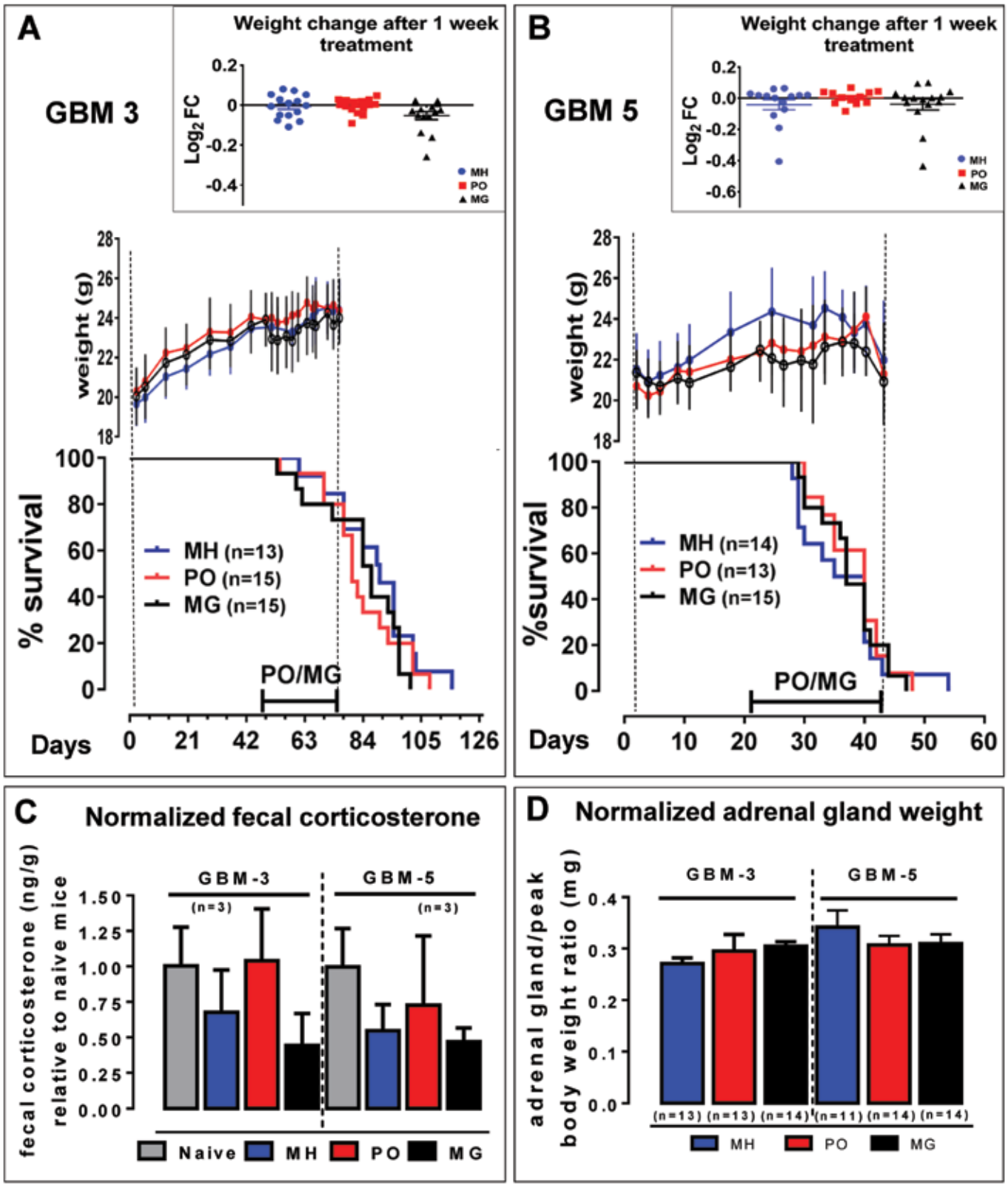

Figure 5. Assessment of physiologic stress elicited by oral gavage. The effect of stress from either daily predator odor (PO) or mock gavage (MG) on body weight changes, survival, excreted corticosterone, and adrenal gland weight were compared with a minimally handled control group (MH). (A) GBM3 PDOX survival was not significantly affected by PO or MG compared with the MH group (log-rank test, $P = 0.3016$ and 0.2755, respectively). Mean body weight periodic measurements are shown for each group until the end of treatment. The insert shows the log2 fold-change for each mouse after 1 wk of treatment, relative to the weight immediately before treatment. Values compared by 1-way ANOVA were not significant ($P = 0.0548$). (B)

vessels,[27] and (very rarely) ventricular involvement.[21,25,32] The PDOX in this study could be divided into 3 groups, according to anatomic location of the terminal tumor: 1) single tumor mass extending from the subcortical areas into the cortex; 2) small multifocal tumors associated with the lateral and third ventricles; and 3) presence of ventricular tumors and diffuse tumor cells in the adjacent subcortical areas. Human glioblastoma tumors have similarly been classified into categories according to MR images that show SVZ or cortical association.[17] The SVZ-associated human tumors were more likely to present multifocal tumors, rapid progression, and decreased survival.[17,26] In addition, in human patients, tumor spread into the ventricles often leads to blockage, resulting in ventricular enlargement, hydrocephalus, and subtotal resection, among other complications.[21,25,39] Recent evidence suggests increased frequency of ventricular involvement for isocitrate dehydrogenase 1 mutant glioblastoma in younger patients,[2] so it is relevant to highlight that the glioblastoma tumors used in this study are wildtype for this enzyme. The free-hand implantation method allows for appropriate control of placement of the injection, with the advantage of higher throughput and minimal restraint compared with stereotactic surgery, enabling the implantation of large cohorts of mice necessary in multi-arm preclinical studies.[3,9,33] We optimized the coordinates for placement of the human tumor cell suspension in a location that promotes cortical tumor growth, avoiding ventricular tumors, as for clinically relevant glioblastoma mouse models, ventricular tumors are not the ideal representation of the human counterpart. The optimal implantation site that we identified here (L4 implantation coordinates ML, –2.5; AP, –1; DV, –3.0) is specific for the mouse strain and age used in our studies. Optimal implantation location must be determined for different strains and age.

Stress has been shown to activate the HPA axis, ultimately resulting in the release of glucocorticoids from the adrenal cortex.[30] This stress response may lead to reduced body weight or, conversely, to body weight gain as well as reduced food consumption and general activity level. In addition, thymus and spleen weights may be reduced whereas adrenal weights may be increased.[6] Stressors activate the sympathetic nervous system leading to release of epinephrine and norepinephrine increasing tumor burden and invasive growth in mouse models of ovarian carcinoma,[43] and prostate cancer.[10] In the current study, we compared the effects of exposure of female nude mice bearing intracranial tumors to daily PO or MG for 4 wk, using a minimally handled untreated cohort as control for stress. Results indicate that MG and PO did not affect several physiologic measurements of stress (body weight, fecal corticosterone, and adrenal gland size), and had no significant effect on tumor growth rate or PDOX overall survival. The reduced HPA axis response observed for athymic mice,[7] along with habituation and a reduced hormonal response from repeated exposure to stress,[42] are likely contributing factors to the lack of detectable stress response observed in this study. With relevance for preclinical research, we conclude that experimental manipulations used in routine oral drug administration regimens for PDOX, as simulated in this study, do not represent a significant stressor, nor do they alter the outcomes of glioblastoma tumor growth in female athymic nude mice.

Our study demonstrates the importance of optimization of preclinical models of human disease, which directly affects the relevance of the model. Optimizing the location of the implantation location for glioblastoma tumor growth, specific for each mouse strain and age, will yield a more consistent and reproducible glioblastoma PDOX for preclinical studies and molecular analysis, increasing the translational value of these models in the development of therapies for glioblastoma.

Acknowledgments

We thank Dr Jennifer C Smith for critical reading of an earlier version of the manuscript. This work was supported by the LIGHT Research Program at the Hermelin Brain Tumor Center and by the NIH (grant no. P01CA085878).

References

1. **Balcombe JP, Barnard ND, Sandusky C**. 2004. Laboratory routines cause animal stress. Contemp Top Lab Anim Sci **43:**42–51.
2. **Ben Nsir A, Gdoura Y, Thai QA, Zhani Kassar A, Hattab N, Jemel H.** 2016. Intraventricular Glioblastomas. World Neurosurg **88:**126–131.
3. **Berezovsky AD, Poisson LM, Cherba D, Webb CP, Transou AD, Lemke NW, Hong X, Hasselbach LA, Irtenkauf SM, Mikkelsen T, Decarvalho AC.** 2014. Sox2 promotes malignancy in glioblastoma by regulating plasticity and astrocytic differentiation. Neoplasia **16:**193–206.
4. **deCarvalho AC, Hoon K, Poisson LM, Winn ME, Mueller C, Cherba D, Koeman J, Seth S, Protopopov A, Felicella M, Zheng S, Zhang J, Petricoin EF, Chin L,Mikkelsen T, Verhaak R.** 2016. Extrachromosal DNA elements can drive disease evolution in glioblastoma. bioRxiv doi:10.1101/081158. [Epub ahead of print].
5. **deCarvalho AC, Nelson K, Lemke N, Lehman NL, Arbab AS, Kalkanis S, Mikkelsen T.** 2010. Gliosarcoma stem cells undergo glial and mesenchymal differentiation in vivo. Stem Cells **28:**181–190.
6. **Everds NE, Snyder PW, Bailey KL, Bolon B, Creasy DM, Foley GL, Rosol TJ, Sellers T.** 2013. Interpreting stress responses during routine toxicity studies: a review of the biology, impact, and assessment. Toxicol Pathol **41:**560–614.
7. **Gaillard RC, Daneva T, Hadid R, Muller K, Spinedi E.** 1998. The hypothalamo–pituitary–adrenal axis of athymic Swiss nude mice. The implications of T lymphocytes in the ACTH release from immune cells. Ann N Y Acad Sci **840:**480–490.
8. **Galli R, Binda E, Orfanelli U, Cipelletti B, Gritti A, De Vitis S, Fiocco R, Foroni C, Dimeco F, Vescovi A.** 2004. Isolation and characterization of tumorigenic, stem-like neural precursors from human glioblastoma. Cancer Res **64:**7011–7021.
9. **Hadaczek P, Ozawa T, Soroceanu L, Yoshida Y, Matlaf L, Singer E, Fiallos E, James CD, Cobbs CS.** 2013. Cidofovir: a novel antitumor agent for glioblastoma. Clin Cancer Res **19:**6473–6483.

Similar to GBM3, GBM5 PDOX overall survival was not significantly affected by PO or MG relative to the MH group (log-rank $P = 0.5684$ and 0.7483 respectively). Mean body weight periodic measurements are shown for each group until the end of treatment. Weights for all groups began to decline simultaneously as result of tumor burden leading to euthanasia. The insert shows the log2 fold-change for each mouse after 1 wk treatment, relative to the weight immediately before treatment. Values compared by 1-way ANOVA were not significant ($P = 0.5347$). (C) The levels of corticosterone were measured by ELISA in fecal samples from GBM3 and GBM5 mice collected over a 24-h period, after 1 wk of treatment, or from nonimplanted naïve mice. Corticosterone levels (ng/g feces) normalized to those from the naïve mice were compared by 1-way ANOVA and were not significantly different among the experimental groups for GBM3 and GBM5 ($P = 0.1103$ and $P = 0.2132$, respectively). (D) At the end of the study, adrenal gland weight was measured and normalized to the peak body weight for each mouse, for the indicated number of subjects per group. Data are reported as mean ± SEM; 1-way ANOVA yielded no significant difference among groups for GBM3 or GBM5 ($P = 0.4587$ and $P = 0.5078$, respectively).

10. **Hassan S, Karpova Y, Baiz D, Yancey D, Pullikuth A, Flores A, Register T, Cline JM, D'Agostino R Jr, Danial N, Datta SR, Kulik G.** 2013. Behavioral stress accelerates prostate cancer development in mice. J Clin Invest **123:**874–886.
11. **Hasselbach LA, Irtenkauf SM, Lemke NW, Nelson KK, Berezovsky AD, Carlton ET, Transou AD, Mikkelsen T, Decarvalho AC.** 2014. Optimization of high grade glioma cell culture from surgical specimens for use in clinically relevant animal models and 3D immunochemistry. J Vis Exp **83:**1–9.
12. **Herter-Sprie GS, Kung AL, Wong KK.** 2013. New cast for a new era: preclinical cancer drug development revisited. J Clin Invest **123:**3639–3645.
13. **Hoffman RM.** 2015. Patient-derived orthotopic xenografts: better mimic of metastasis than subcutaneous xenografts. Nat Rev Cancer **15:**451–452.
14. **Ignatova TN, Kukekov VG, Laywell ED, Suslov ON, Vrionis FD, Steindler DA.** 2002. Human cortical glial tumors contain neural stem-like cells expressing astroglial and neuronal markers in vitro. Glia **39:**193–206.
15. **Inda MM, Bonavia R, Seoane J.** 2014. Glioblastoma multiforme: a look inside its heterogeneous nature. Cancers (Basel) **6:**226–239.
16. **Institute for Laboratory Animal Research.** 2011. Guide for the care and use of laboratory animals, 8th ed. Washington (DC): National Academic Press.
17. **Jafri NF, Clarke JL, Weinberg V, Barani IJ, Cha S.** 2013. Relationship of glioblastoma multiforme to the subventricular zone is associated with survival. Neuro Oncol **15:**91–96.
18. **Jain RK, di Tomaso E, Duda DG, Loeffler JS, Sorensen AG, Batchelor TT.** 2007. Angiogenesis in brain tumours. Nat Rev Neurosci **8:**610–622.
19. **Jeong JY, Lee DH, Kang SS.** 2013. Effects of chronic restraint stress on body weight, food intake, and hypothalamic gene expressions in mice. Endocrinol Metab (Seoul) **28:**288–296.
20. **Kapelewski CH, Bennett JM, Cavigelli SA, Klein LC.** 2010. Application of a naturalistic psychogenic stressor in periadolescent mice: effect on serum corticosterone levels differs by strain but not sex. BMC Res Notes **3:**170.
21. **Kim YJ, Lee SK, Cho MK, Kim YJ.** 2008. Intraventricular glioblastoma multiforme with previous history of intracerebral hemorrhage: a case report. J Korean Neurosurg Soc **44:**405–408.
22. **Laks DR, Masterman-Smith M, Visnyei K, Angenieux B, Orozco NM, Foran I, Yong WH, Vinters HV, Liau LM, Lazareff JA, Mischel PS, Cloughesy TF, Horvath S, Kornblum HI.** 2009. Neurosphere formation is an independent predictor of clinical outcome in malignant glioma. Stem Cells **27:**980–987.
23. **Larjavaara S, Mantyla R, Salminen T, Haapasalo H, Raitanen J, Jaaskelainen J, Auvinen A.** 2007. Incidence of gliomas by anatomic location. Neuro Oncol **9:**319–325.
24. **Lee J, Kotliarova S, Kotliarov Y, Li A, Su Q, Donin NM, Pastorino S, Purow BW, Christopher N, Zhang W, Park JK, Fine HA.** 2006. Tumor stem cells derived from glioblastomas cultured in bFGF and EGF more closely mirror the phenotype and genotype of primary tumors than do serum-cultured cell lines. Cancer Cell **9:**391–403.
25. **Lee TT, Manzano GR.** 1997. Third ventricular glioblastoma multiforme: case report. Neurosurg Rev **20:**291–294.
26. **Lim DA, Cha S, Mayo MC, Chen MH, Keles E, VandenBerg S, Berger MS.** 2007. Relationship of glioblastoma multiforme to neural stem cell regions predicts invasive and multifocal tumor phenotype. Neuro-oncol **9:**424–429.
27. **Louis DN, Perry A, Reifenberger G, von Deimling A, Figarella-Branger D, Cavenee WK, Ohgaki H, Wiestler OD, Kleihues P, Ellison DW.** 2016. The 2016 World Health Organization classification of tumors of the central nervous system: a summary. Acta Neuropathol **131:**803–820.
28. **Lutterbach J, Guttenberger R, Pagenstecher A**. 2001. Gliosarcoma: a clinical study. Radiother Oncol **61:**57–64.
29. **Moreno-Smith M, Lutgendorf SK, Sood AK.** 2010. Impact of stress on cancer metastasis. Future Oncol **6:**1863–1881.
30. **Nagaraja AS, Armaiz-Pena GN, Lutgendorf SK, Sood AK.** 2013. Why stress is BAD for cancer patients. J Clin Invest **123:**558–560.
31. **Office of Laboratory Animal Welfare.** 2015. Public health service policy on humane care and use of laboratory animals. Bethesda (MD): National Institutes of Health.
32. **Ostrom QT, Gittleman H, Fulop J, Liu M, Blanda R, Kromer C, Wolinsky Y, Kruchko C, Barnholtz-Sloan JS.** 2015. CBTRUS statistical report: primary brain and central nervous system tumors diagnosed in the United States in 2008 to 2012. Neuro Oncol **17 Suppl 4:**iv1–iv62.
33. **Ozawa T, James CD.** 2010. Establishing intracranial brain tumor xenografts with subsequent analysis of tumor growth and response to therapy using bioluminescence imaging. J Vis Exp **41:**1986.
34. **Patil CG, Yi A, Elramsisy A, Hu J, Mukherjee D, Irvin DK, Yu JS, Bannykh SI, Black KL, Nuno M.** 2012. Prognosis of patients with multifocal glioblastoma: a case-control study. J Neurosurg **117:**705–711.
35. **Paxinos G, Franklin KBJ.** 2013. The mouse brain in stereotaxic coordinates. New York (NY): Elsevier.
36. **Reynolds BA, Weiss S.** 1992. Generation of neurons and astrocytes from isolated cells of the adult mammalian central nervous system. Science **255:**1707–1710.
37. **Rygaard J, Povlsen CO.** 1969. Heterotransplantation of a human malignant tumour to "Nude" mice. Acta Pathol Microbiol Scand **77:**758–760.
38. **Schneider CA, Rasband WS, Eliceiri KW.** 2012. NIH Image to ImageJ: 25 years of image analysis. Nat Methods **9:**671–675.
39. **Secer HI, Dinc C, Anik I, Duz B, Gonul E.** 2009. Glioblastoma multiforme of the lateral ventricle: report of 9 cases. Br J Neurosurg **22:**398–401.
40. **Sharkey FE, Fogh J.** 1984. Considerations in the use of nude mice for cancer research. Cancer Metastasis Rev **3:**341–360.
41. **Sundbom R, Jacobsen KR, Kalliokoski O, Hau J, Abelson KS.** 2011. Postoperative corticosterone levels in plasma and feces of mice subjected to permanent catheterization and automated blood sampling. In Vivo **25:**335–342.
42. **Sutanto W, de Kloet ER.** 1994. The use of various animal models in the study of stress and stress-related phenomena. Lab Anim **28:**293–306.
43. **Thaker PH, Han LY, Kamat AA, Arevalo JM, Takahashi R, Lu C, Jennings NB, Armaiz-Pena G, Bankson JA, Ravoori M, Merritt WM, Lin YG, Mangala LS, Kim TJ, Coleman RL, Landen CN, Li Y, Felix E, Sanguino AM, Newman RA, Lloyd M, Gershenson DM, Kundra V, Lopez-Berestein G, Lutgendorf SK, Cole SW, Sood AK.** 2006. Chronic stress promotes tumor growth and angiogenesis in a mouse model of ovarian carcinoma. Nat Med **12:**939–944.
44. **Touma C, Palme R, Sachser N.** 2004. Analyzing corticosterone metabolites in fecal samples of mice: a noninvasive technique to monitor stress hormones. Horm Behav **45:**10–22.
45. **Vescovi AL, Galli R, Reynolds BA.** 2006. Brain tumour stem cells. Nat Rev Cancer **6:**425–436.
46. **Walker MK, Boberg JR, Walsh MT, Wolf V, Trujillo A, Duke MS, Palme R, Felton LA.** 2012. A less stressful alternative to oral gavage for pharmacological and toxicological studies in mice. Toxicol Appl Pharmacol **260:**65–69.
47. **Yang L, Lin C, Wang L, Guo H, Wang X.** 2012. Hypoxia and hypoxia-inducible factors in glioblastoma multiforme progression and therapeutic implications. Exp Cell Res **318:**2417–2426.